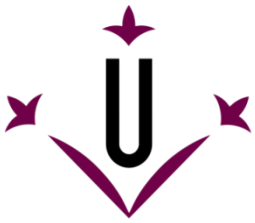

Standardisation of near infrared hyperspectral imaging for quantification and classification of DON contaminated wheat samples

Antoni Femenias[a], Ferran Gatius[b], Antonio J. Ramos[a], Vicente Sanchis[a], Sonia Marín[a,*]

[a]Applied Mycology Unit, Food Technology Department, University of Lleida, UTPV-XaRTA, AGROTECNIO, Av. Rovira Roure 191, 25198, Lleida, Spain

[b]Department of Chemistry, University of Lleida (UdL), Av. Rovira Roure, 191, Lleida, 25198, Spain

Corresponding author:

Sonia Marín Sillue

Food Technology Department, University of Lleida

Av. Rovira Roure 191, 25198, Lleida, Spain

Tel: (+34) 973 70 25 42

Fax: (+34) 973 70 25 96

Email: smarin@tecal.udl.cat

ABSTRACT

Near infrared hyperspectral imaging (HSI-NIR) is considered a promising technique able to replace time-consuming, costly and destructive classic methods to predict and classify deoxynivalenol (DON) contaminated wheat kernels or samples by its concentration and level of contamination, respectively. The main objective of the present study was to standardise the HSI-NIR image acquisition method in naturally contaminated whole wheat kernels to obtain a high accuracy method to quantify and classify samples according to DON levels. To confirm the results, wheat samples were analysed by high performance liquid chromatography as the reference method to determine their DON levels. Hyperspectral images for single kernels and whole samples were obtained and spectral data were processed by multivariate analysis software. The initial work revealed that HSI-NIR was able to overcome kernel orientation, position and pixel selection. The subsequent developed Partial Least Squares (PLS) prediction achieved a RMSEP (Root Mean Square Error of Prediction) of 405 µg/kg and 1174 µg/kg for a cross-validated model and an independent set validated model, respectively. Moreover, the classification accuracy obtained by Linear Discriminant Analysis (LDA) was 62.7% for two categories depending on the UE maximum level (1250 µg/kg). Despite of the results are not accurate enough for DON quantification and sample classification, they can be considered a starting point for further improved protocols for DON management.

1. INTRODUCTION

Deoxynivalenol (DON) is a *Fusarium* produced mycotoxin causing increasing concern due to its prevalence in wheat. European diet is highly based on wheat derivatives, thus exposure to DON may be significant (Cano-Sancho et al., 2011). There is a highly seasonal variation in *Fusarium* mycotoxins in wheat, and the agronomic factors should be taken into account to minimise *Fusarium* mycotoxin levels in harvested wheat. *Fusarium graminearum*, a major DON producer, invades the spikelets, causing kernel damage in the form of shrivelling appearance, loss of weight, and discoloration that results in a white or pink appearance (Delwiche, Kim, & Dong, 2010). Although different preharvest strategies have been applied to minimise DON presence in wheat, the problem still remains (Edwards & Jennings, 2018). Moreover, DON is not fully destroyed by any of the food processing methods (Vidal, Sanchis, Ramos, & Marin, 2016). As a consequence, monitoring of wheat batches prior entering the food chain is a key point in order to divert highly contaminated batches.

Several laboratory methods are available for detection and measurement of DON in cereal grains, including high performance liquid chromatography, mass spectrometry, and enzyme-linked immunosorbent assays. However, these methods are not suitable for rapid detection at the entry in food industries. At the moment, companies that monitor all entering batches use lateral flow devices for rapid screenings, despite they have limited accuracy. To date, there is a high interest to apply the spectroscopic detection techniques for the identification of DON contaminated samples. Spectroscopic detection techniques are already widely used in food and feed industries for the determination of organic compounds in matter, like proteins,

moisture, starch and pigments. The relatively low concentration range for DON makes it very challenging for NIR quantitative analysis. As an alternative to measurement of DON, some NIR studies have relied on the positive, though imperfect correlation between the visual appearance of *Fusarium* damage and DON (Delwiche et al., 2010). For the NIR region, the spectral absorption near 1200 nm, attributed to ergosterol, has been shown to be useful in spectral recognition of *Fusarium* damage (Delwiche, Kim, & Dong, 2011). In particular, Fourier transform near- and mid-infrared (FT-NIR and FT-MIR) spectroscopy has been successfully used for the detection of DON in 30 g (De Girolamo, Cervellieri, Visconti, & Pascale, 2014) and 25 g (Dvořáček, Prohasková, Chrpová, & Štočková, 2012) of wheat. This has allowed classification of samples according to their level of contamination, although some studies used highly artificially contaminated ones, and in some cases milling of the samples was required before spectroscopic measurements. This technology is based on interferometry, as opposed to the grating-based ones, producing better resolution and throughput.

Hyperspectral imaging (HSI) combined with spectroscopy represents a new non-destructive methodology. Its advantage is that it provides spectral information at each spatial pixel on a sample, thus ensuring higher analytical potential (Cen, Lu, Zhu, & Mendoza, 2016). Most common HSI methods are using diffraction gratings based on the instantaneous acquisition of spectra. The push-broom method is the most widely spread method within the market of HSI cameras. It consists in an instantaneous acquisition of a spatial line (x) and the whole lambda range. Only the 'y' dimension has to be scanned over time (Photon lines S.L., 2016). Studies of HSI-NIR technology application to detect quality parameters in cereals (Caporaso, Whitworth, & Fisk, 2018), to asses *Fusarium* and DON in wheat kernels (Femenias, Gatius, Ramos, Sanchis, & Marín, 2020) and to detect mycotoxins and mycotoxigenic fungi in food products (Xing et al., 2019) have been reviewed.

HSI-NIR has been already proposed by some authors for assessment of *Fusarium*-damaged kernels percentage and DON presence at given levels. Delwiche et al. (2010, 2011) studies used visual inspection as a reference method to classify 60 kernels for sample by Linear Discriminant Analysis (LDA) according to Fusarium Head Blight (FHB) presence. Moreover, Shahin & Symons (2011, 2012) and Delwiche, Rodriguez, Rausch & Graybosch (2019) also aimed to classify a larger number of *Fusarium*-Damaged Kernels (FDK) by LDA and Partial Least Squares-Discriminant Analysis (PLS-DA). All these authors reduced the dimensionality of the data by the selection of characteristic wavelengths for FDK. However, the symptomatology of kernels cannot be totally related with DON presence, so that some asymptomatic kernels can contain DON and vice versa (Barbedo, Tibola, & Fernandes, 2015). The relationship between DON concentrations and *Fusarium* is stronger

for high DON levels and weaker for lower DON concentrations. Thus, some error is inevitable because at low DON concentrations, typical *Fusarium* damage symptoms are not visually detectable. Moreover, at high DON contaminations, the correlation is stronger and consequently higher percentage of damaged kernels can be observed (Beyer, Klix, & Verreet, 2007). Therefore, HIS-NIR technique is proposed to overcome visual symptoms disassociations with DON contamination.

Moreover, Barbedo, Tibola, & Lima (2017) used a confusion matrix to classify DON contaminated kernels into three groups: below 500 µg/kg, between 500 and 1250 µg/kg and above 1250 µg/kg (legal UE limit) and Liang et al. (2018) developed a complex method based on Support Vector Machine (SVM) and PLS-DA to classify at three DON levels with mean values of <250, 1162 and 2665 µg/kg.

The present article aims to standardise the methodology used for HSI-NIR image acquisition in whole wheat kernels, in order to have a precise method to screen samples for DON presence. Once standardised, the protocol was used for an attempt to quantify DON level through PLS regression. Moreover, 150 naturally contaminated samples were scanned and classified according to the maximum limit in the EU (1250 µg/kg).

2. MATERIALS AND METHODS

2.1 Determination of DON concentration in wheat samples by UHPLC

2.1.1 Reagents and chemicals

Water was obtained from a Milli-Q® SP Reagent water system from Millipore Corp. (Brussels, Belgium). Methanol and acetonitrile (HPLC grade) were purchased from Scharlab (Sentmenat, Spain). Mycotoxin standards of DON were purchased from Romer Labs (Tulln, Austria). Immunoaffinity columns (IAC) for DON (DONPREP®) were acquired from R-Biopharm (Rhone LTD Glasgow, UK).

2.1.2 Preparation of DON solutions

DON concentration in the stock solution was checked by UV spectroscopy according to AOAC Official Methods of Analysis, Chapter 49 (AOAC, 2005), obtaining a concentration of the stock solution of 791 µg/mL. Standard solutions of DON were prepared in methanol at a concentration of 9.55 µg/mL and stored at 4 °C. Calibration curves were prepared by appropriate dilution of known volumes of the stock solution with the mobile phase.

2.1.3 DON extraction in wheat

A total of 150 wheat samples were supplied by a feed producing agricultural cooperative (Cotécnica S.C.C.L, Bellpuig, Lleida, Spain). Their origin was Lleida province. They were taken within its quality control programme from each incoming truck. From the whole homogenized sample, a subsample (200-500 g) was sent to our laboratory.

DON was extracted using specific immunoaffinity columns (DONPREP®) following the manufacturer's instructions. The mycotoxin extraction followed a slightly modified version of the methodology used by Vidal, Sanchis, Ramos, & Marín (2018). Briefly, five grams of wheat previously ground with an IKA® A11 Basic mill (Darmstadt, Germany) were mixed with 30 mL of MiliQ water in a 250 mL Erlenmeyer flask, followed by 10 min stirring. Then, samples were centrifuged for 10 min at 1780×g. Supernatant was filtered through a 9 mm of diameter glass microfiber paper filter (Whatman™ GF/A, Maidstone, UK) and 5 mL of the filtrate was passed through the immunoaffinity column. The column was then washed with 10 mL of bi-distilled water and the toxins were eluted with 3 mL of methanol HPLC-grade (the first 1.5 mL performing back-flushing). Samples were evaporated under a low nitrogen stream at 40 °C and resuspended in the mobile phase (acetonitrile:methanol:water, 5:5:90, v/v/v). Every resuspended extract was filtered through a nylon filter (0.4µm) before being injected into the UHPLC-DAD system.

2.1.4 UHPLC system

The determination of DON was performed using an Agilent Technologies 1260 Infinity UHPLC system (California, USA) coupled with an Agilent 1260 Infinity II Diode Array Detector (DAD). A Gemini® C18 column from Phenomenex 150×4.6 mm (California, USA) with a particle size of 5 µm and a pore size of 110 Å was used. Absorption wavelength was set at 220 nm. The mobile phase was composed of methanol:acetonitrile:water (5:5:90, v/v/v) and set at a flow rate of 1 mL/min. The column temperature was 40 °C, the injection volume was 50 µL and total run time was 15 min for mycotoxin analyses. The performance of the method for the quantification of DON in wheat was previously published in Vidal et al. (2018), in which the limit of detection (LOD) was considered to be three times the signal of the blank (50 µg/kg).

2.2 HIS-NIR experimental work

2.2.1 Instrumentation and data acquisition by HSI-NIR

A push-broom hyperspectral imaging system composed by a Pika NIR-320 camera assembled in RESONON Inc. (Boezman, MA, USA) was used. The device consists in an InGaAS sensor line scan camera with 320×256-pixel resolution, a 30×30 µm pixel size, a 14-bit resolution A/D

spectrograph (Goldeye G-008 SWIR TEC1, Allied Vision Technologies GmbH, Germany). The spectral resolution is 4.9 nm (164 spectral bands from 900 to 1700 nm), with 320 pixels of spatial resolution and frame rate of 520 fps. The objective lens has 25 mm of focal length (F/1.4 SWIR, 0.9-1.7 µm, 21mm image format, c-mount) and are positioned 220 mm above the image surface. Illumination unit is composed by a four halogen lamps lighting system with Lambertian filters fixed on an adjustable tower that are turned on at least 20 min before the image acquisition. The illumination system was powered by Samplexpower® power converter (SEC-1223CE, Burnaby, BC, V5A 0C6, Canada) which provides a highly regulated output DC voltage of 13.8 Volts at 23 Amps with an AC input of 230 Volts, 50 Hz. Finally, a motorized linear translation stage of 600 mm was also used, which permitted the scan of the full sample having the optical systems fixed.

The Spectronon PRO software was used to control Resonon's benchtop for the image processing. The intensity readings of each test sample data array were automatically transformed to reflectance by dividing the dark current-subtracted intensity by the dark current-subtracted white standard intensity at each of the corresponding wavelengths (1). A dark current intensity image was collected before samples' scanning to remove dark current noise by covering the camera lens. Likewise, intensity from a 99% reflectance standard, made of PTFE (Spectralon™, SRT-99-120, Labsphere, North Sutton, NH, USA) to correct illumination effects, was collected immediately after the dark current image. These two images were applied to the subsequent sample intensity images.

$$I = \frac{I_0 - I_b}{I_w - I_b} \quad (1)$$

where I_0 is the raw hyperspectral image obtained, I_w is the white reference and I_b is the dark current reference. In addition to dark and absolute reflectance response, the pixel illumination saturation was also adjusted by the camera controls. Framerate and integration time were established so that no pixel on the image was saturated.

The work was divided in three parts, in the first preliminary one, pixel selection, kernel location and repeatability were evaluated by acquiring images of 30 individual kernels (from uncontaminated samples) placed crease-down in a template as shown in Fig. 1a. Mean spectrum for each kernel was recorded. In the second part, kernel orientation and data preprocessing were evaluated by acquiring images of 30 individual kernels (from both contaminated and uncontaminated samples) placed crease-down in a template (Fig. 1a). Mean spectrum for each kernel was recorded. In the third part, for bulk sample analysis, approximately 7 g of wheat kernels were scanned without any specific template as in Fig. 1b and the mean spectrum of the whole image was recorded. In all three parts, a black tray

was used to reduce the background noise on the image and to obtain an accurate pixel selection. Images were adjusted to 350 bands for horizontal size and approximately 90 mm of vertical size. The pixel selection was done by the collection of the mean reflectance's of similar spectrum pixels by Euclidian distance that are best adjusted to the region of interest (ROI) to remove the background signal. Mean spectra for each kernel and for full samples were recorded as text file for their subsequent exporting to the spectral analysis software.

2.2.2 Hyperspectral data processing for preliminary work

Spectral data were processed using The Unscrambler software (version 7.6 SR1, CAMO, Oslo, Norway, 2001). For preliminary work with uncontaminated samples, Principal Component Analysis (PCA) projections were performed on the mean spectra without spectral data preprocessing. The purpose of PCA was to identify the variations between different sampling conditions by highlighting valuable information from the spectral data. First, to compare the differences between the selection mode, either restrictive (avoiding any pixels from the background) or permissive (extending the selection to all kernel pixels, thus including some from the background), the same sample was selected in both modes and spectra compared using PCA. Second, PCA was also used to determine the influence of the kernel position on the scanning tray. To evaluate this effect, 30 crease down kernels were located on different positions for each of the three images captured, as shown in the Fig. 2. Finally, the repeatability of the image acquisition was also evaluated by PCA, by scanning 5 samples in 3 consecutive days (different calibrations of the equipment).

2.2.3 Hyperspectral data processing for tests with DON-contaminated and uncontaminated samples

The spectral profile of the mean raw spectra of kernels from non-contaminated (<LOD), midly-contaminated (1605.9 μg/kg) and highly contaminated (2682.8 μg/kg) samples was determined by a line plot representation of the reflectance spectra. Spectral preprocessing algorithms were tested to determine the pretreatment which best fits to the raw data obtained. First, the transformation of the reflectance data to absorbance spectra was introduced using the spectroscopic transformation tool from The Unscrambler software. Second, baseline correction, in which the lowest value was subtracted from all the remaining values in the spectrum, was applied to both reflectance and absorbance spectra. Third, a standard normal variate (SNV) transformation was applied to both spectra. The evaluation of the best pretreatment was achieved also by PCA.

In addition, the effect of the orientation about the kernel axis (crease up and down) was assessed. Images of both orientations for each kernel by rotating on themselves were captured. The differences in their spectra were estimated for both DON contaminated and non-contaminated samples by PCA projection with the most suitable pretreatment applied. The comparison between DON-effect and kernel orientation on the PCA was done employing kernels from samples contaminated at 2190, 2682.8 and 2882 μg/kg paired in each case with kernels from samples with DON concentration below the LOD.

Moreover, kernels from DON-contaminated and uncontaminated samples were classified according to the typical symptoms caused by *Fusarium* infection by a visual inspection (eg. discoloration, wrinkles, wilting and dwarfing). Visually sound kernels were defined as round, large and brownish. Both types of grains were scanned and the resulting spectra were preprocessed according to the best pretreatment. Preprocessed spectra were modelled by PCA for the evaluation of the relationship between symptomatology and DON contamination.

2.3 Hyperspectral data processing for quantification and classification of bulk DON contaminated samples

Firstly, the within sample repeatability was assessed by sampling for three times approximately 7 g of grain from the same sample, so that different kernels from the same sample were evaluated. Kernels arising from four samples considered contaminated (2681 μg/kg and 1770 μg/kg), midly-contaminated (660 μg/kg) and uncontaminated (<LOD) were scanned in triplicate, so that a total of 36 images and 12 mean spectra were acquired. The kernels were not separated from each other, so they overlapped on the image. The spectral processing was done applying the formerly selected spectral pretreatment followed by a PCA model.

The prediction model was built by recording pixels mean reflectances along wavelength of 7 g from 74 samples covering the DON concentration range from <LOD to 2660.0 μg/kg as explanatory variables, and DON concentration obtained by UHPLC as dependent variable. A total of 222 images (74 samples in triplicate) were obtained to develop a cross-validated model. The same samples were divided in two sets, in which kernels arising from 24 samples were scanned (72 images) for the calibration set and kernels from 50 samples (150 images) for the validation set, shaking them between scans to randomly distribute the kernels and to obtain a major representativeness of the spectra. Mean spectra were calculated from the pixel spectra of all scanned kernels. Triplicate spectra were treated independently to introduce a total of 222 observations in the multivariate analysis tool (The

Unscrambler 7.6 SR1). The reflectances were transformed to absorbances and a baseline correction offset (subtracting the minimum value to the entire spectrum) was applied. A PLS was constructed and refined in order to simplify the model. Two prediction models were performed. The first regression model used a full cross-validation to obtain the best RMSECV (Root Mean Square Error of Cross-Validation) as possible. The second one used the two divided sample sets, in order to obtain the prediction performance with the RMSEP (Root Mean Square Error of Prediction). A total of 22 from 220 spectra were removed as they were considered outliers for the cross-validated model. Only 3 outliers were removed for the test set validated model. The criteria followed for outlier detection was to represent the influence plot, and reject those spectra with higher leverage and residual Y-variance. Less than the 10% of the original spectra were removed. The criteria used to select the number of PCs to optimize the models (for cross-validation and for test set) was the PC number where the first minimum on the curve of the Root Mean Square Error (RMSE) occurs. Validation accuracy was assessed by the performance parameters, that is, the slope, correlation, coefficient of determination, RMSEP and SEP.

The classification model was developed using the data in the validation set of the preceding PLS model, that is 150 images from 50 samples at different concentrations. The images were distributed into two sets, each of them covering the widest range of concentrations as possible. Statistical analysis was performed with JMP PRO 14.1.0 (SAS Institute Inc., 2018) software using Linear Discriminant Analysis (LDA) model able to characterize two or more classes, first by a dimensionality reduction step and a second classification stage. The limit established for the two classes separation was the EU legal limit for DON (1250 µg/kg). From the 75 images used for the calibration and the 75 for the validation set, 47 corresponded to kernels arising from samples below 1250 µg/kg of DON (B) and 28 to kernels from samples above the legal limit (C). Accuracies were obtained as the percentage (%) of correctly classified images from the total (75).

3. RESULTS

3.1 Preliminary work with uncontaminated samples

3.1.1 Image preprocessing: Kernel pixels' selection

The selection tool of the software was used for segmentation of kernels from the background, based on the similar spectra to the chosen pixel. The selection tool not always implies that

exactly the same pixels are selected, because this depends on the pixel chosen. Still the recorded reflectance was quite similar when the pixels of the same kernel were selected twice, for 25 kernels from the same sample placed crease-down captured in a single image. The score plot of the PCA model showed that differences among kernels were much wider than the error caused by the selection tool (Fig. S1, supplementary material).

Moreover, a score plot of the PCA model for the reflectance spectra of the previously used 25 kernels was obtained, for which the region of interest (ROI) for each kernel was selected twice (the first spectra limited to the pixels located within the kernel and the second one including the whole kernel area and, consequently, some background). The differences among kernels were wider than those due to the selection method, but still the difference was important (Fig. S2, supplementary material), thus the narrow selection was chosen for the following steps.

3.1.2 Kernel location on the scanning tray

The PCA projection obtained from the three different images of 30 kernels crease-down placed on different locations on the plate (as explained in methodology) did not display large differences among the three repetitions of the same kernel, as it is shown in the score plot in Fig. 3. This means that radiation reached kernels equally regardless of their location in the tray, and was reflected and measured in a similar manner.

3.1.3 Repeatability of image acquisition

A PCA model showed the differences among sample scans for three different days. Five samples were used to check the possible variances caused by time intervals between analyses. Although different projections were observed for the different days, no score groups for each day were present, thus time was not involved in group formation. In addition, the plot shows a slight grouping for the repeated samples, each one represented with the same colour for the three scores (Fig. S3, supplementary material).

3.2 Tests on DON-contaminated and uncontaminated samples

3.2.1 Spectral profiles of different DON levels

Fig. 4 shows three spectra corresponding to different levels of contamination of 30 kernels placed crease-down in the scanning area. In general, uncontaminated samples showed higher reflectance, however, this point was not confirmed for different samples, thus it was concluded that some kind of data preprocessing was required. In the Fig. 4, the 1200 nm and 1480 nm absorption bands are indicated as they have been related to ergosterol and chitin, respectively (Delwiche et al., 2011, 2019), however, the observed differences were not clearly wider at these wavelengths.

3.2.2 Kernel orientation (crease-down or crease-up)

Comparison of reflectance of kernels rotating on themselves in order to obtain crease-down and crease-up images was achieved for a DON-free and a DON-contaminated sample. In Fig. S4 (supplementary material), the projections for 30 kernels of a non-contaminated sample are represented in the upper part, and for a contaminated sample in the lower part. The dashed line ellipse corresponds to the group where the majority of the crease-up oriented kernels were distributed. Besides, the continuous line ellipse includes the crease-down kernels. Thus PC1 accounted for the differences among kernels (93% of the variability), while the impact of the different orientation appears in the PC2 with lower variability, accounting for less than 7% of the spectral variance.

3.2.3 Spectral data pretreatment determination

A PCA analysis was performed to compare between the different spectral pretreatments applied to the raw data (reflectance spectra) in the ability of HSI-NIR to discriminate DON-contaminated kernels from those under the LOD (Fig. S5 and S6, supplementary material). The PCA score plot corresponds to crease down and crease up kernels scan, respectively. Continuous line ellipses represent the projection area in the score plot for kernels contaminated with 1719.8 μg/kg, while dashed-lines ellipses (dashed-line) correspond to the <LOD kernels. The ellipses showed the groups of kernels for each contamination and, in some cases, are overlapped and some sample appears in the other group. It was concluded that transformation to absorbance plus baseline correction was the best choice, if grains both crease-down and crease-up are to be placed in the scanning area.

3.2.4 Kernel orientation and discrimination of DON contaminated kernels

Fig. 5 shows the comparison of contaminated (C) and non-contaminated (B) kernels placed crease-down (D) or crease-up (V) during the scan. All the following results are obtained from absorbance spectra pretreated with a baseline correction, categorized as the most appropriate adjustment to highlight DON contamination. Each number corresponds to the evaluation of four different samples, three contaminated with DON and one under the LOD. Result 1A depicts 60 wheat kernels from a sample with a DON concentration of 2682.8 μg/kg, result 2A from a sample with 2190.0 μg/kg of DON and finally, result 3A plots the same number of kernels from a sample with 2660.0 μg/kg. Group B kernels came from samples with concentration below the LOD. It is concluded that while separation of grains due to DON-contamination occurs in the PC1 (A figures), no relation exists with the grain orientation (B figures). It was then determined that grains could be placed in the scanning area oriented at random.

3.2.5 Visual symptoms and contaminated kernels detection

A PCA score plot of the combination of two features, DON contamination and kernel symptoms, is presented in Fig. 6. It shows the influence of kernel symptoms (discoloration, wrinkles and wilting) in the discrimination of kernels with and without DON. Contaminated samples contained a larger number of symptomatic kernels than non-contaminated ones. The projection of four different groups, categorized as contaminated and symptomatic (CS), contaminated and asymptomatic (CA), non-contaminated and symptomatic (BS) and non-contaminated and asymptomatic (BA) showed that the separation along PC1 (97% of variability) is due to the difference among symptomatic contaminated kernels from uncontaminated ones (either symptomatic or not). It must be remembered that no confirmation of the DON-contamination at kernel level exists in this study, thus some of the kernels classified as contaminated could be uncontaminated and vice versa. In conclusion, the symptoms of *Fusarium* damage are the basis for the discrimination as expected. Thus the success of the discrimination is directly affected by the correlation between *Fusarium*-DON.

3.3 Quantification and classification models for bulk samples

3.3.1 Repeatability within samples

The different subsamples (7 g) arising from the same bulk sample showed some differences (Fig. 7). PC1 accounted for 100% of spectral data variability, where subsamples <LOD were projected separately on the left, those from the sample contaminated at 660 μg/kg were placed in the middle and those contaminated at 1770 and 2881 μg/kg overlapped on the right, which is quite expectable taking into account the heterogeneous distribution of mycotoxins in particulate commodities.

3.3.2 Calibration of a PLS regression model and validation

The model was based on 200 images (from 24 samples scanned in triplicate) used for the calibration of the PLS model. The model was build up by introducing samples from a contamination range between <LOD and 2660 μg/kg, which includes the legal UE limit (1250 μg/kg). Fig. 8 represents the predicted versus measured values plot in which the blue line corresponds to the predicted regression line obtained from spectral data (by full cross-validation). The statistic parameters for the validation (obtained by full cross-validation) of the calibration model are presented in the Fig. 8. The coefficient of determination (R_{cv}^2) obtained was 0.72, the offset was 249.48, the root mean square error of calibration (RMSECV) was 405.9 μg/kg and the slope was 0.76. The optimum number of PC used for the best adjustment of the regression were 17.

The same samples were evaluated by dividing the images into 72 for the calibration set (24 samples in triplicate) and an independent test set of 150 images (from 50 samples scanned

388 in triplicate). The concentration range used to test the performance of the model was the
389 same used for the cross-validated model. In this case, the statistic parameters obtained by
390 the model based on the test set spectra were a coefficient of determination (R_p^2) of 0.27 an
391 offset of 883.4 μg/kg, a root mean square error of prediction (RMSEP) of 1174.4 μg/kg and
392 a slope of 0.77, which suggested that prediction of DON concentration levels for individual
393 bulk samples was not possible under the conditions tested in this work (Fig. 9).

394 **3.3.3 Classification model**

395 A total of 150 images were divided into two sets of 75 images (training and validation) for a
396 LDA classification. Each set was composed by 47 images corresponding to the B group (grain
397 arising from samples contaminated by DON below 1250 μg/kg) and 28 images corresponding to
398 the group C (above 1250 μg/kg). Table 1 shows the number of correct and misclassified samples
399 for both sets by LDA. The percentage of samples correctly classified was 73.4% (55/75) for the
400 training set and 62.7% (47/75) for the validation set. From the incorrectly classified samples,
401 half of them (19%) were fail-dangerous, which means that they were contaminated over the
402 legal limit, but predicted to be under the limit.

403 **4. DISCUSSION**

404 In the present work a HSI-NIR system was set up for wheat sample images acquisition, and
405 its ability for detection of DON naturally contaminated bulk samples was assessed. In
406 summary, for the setup it was concluded that good repeatability can be expected interday
407 and for repeated scannings of the same sample (even with mixing up of the kernels, as
408 position in the scanning area and orientation of the kernels was confirmed to have low
409 impact on the mean reflectance). FT-NIR has also been used to screen bulk samples.
410 Published studies used high DON levels, much above those considered as safe, except for
411 De Girolamo, Lippolis, Nordkvist, & Visconti (2009) and De Girolamo, Cervellieri,
412 Visconti, & Pascale (2014) who worked in naturally contaminated samples (ground
413 samples) with a DON range of 50-2600 μg/kg and <50-16,000 μg/kg, the last one so far to
414 the present study. In comparison with De Girolamo et al. (2009), our study achieved a slope
415 of 0.85 for the cross-validated model, slightly better than the 0.83 obtained the
416 abovementioned author. Otherwise, the coefficient of determination obtained was slightly
417 lower (0.72) than achieved in previous studies (0.82). Additionally, the RMSECV obtained
418 in this study was better (405.9 μg/kg) in comparison with the error obtained in the previous
419 one (516 μg/kg). However, in the present study 17 latent variables (LV) were used, so the
420 model obtained was more complex than in the two compared study (4). Our independent
421 validation set model presented poorer results for the model adjustment, obtaining a

correlation of 0.52 in comparison with the 0.79 achieved by both studies. In addition, we obtained an r^2 value of 0.27, lower than the 0.63 from both compared studies. However, our RMSEP achieved for the validation set (1,174.6 µg/kg) is comparable to the lower error (868.0 µg/kg) obtained by De Girolamo et al. (2009) and the higher (1977.0 µg/kg) obtained by De Girolamo et al. (2014) in which only 8 LV were needed. Our r^2 describes a weak adjustment, but we obtained a level of significance lower than 0.05 for the analysis of variance of the regression predicted values vs the observed ones, so we can affirm that there is a linear relation between both measures and that the difference between the real and the obtained values is not due to random error Nevertheless, our SEP (979.3 µg/kg) was extensively lower than that of the validated model of Peiris, Dong, Bockus & Dowell (2013) by FT-NIR in bulk grain samples, which was 2,400 µg/kg. The difference in the errors of prediction between studies could be due to wider range of concentrations used in previous studies (<50-3,000 µg/kg; <50-16,000 µg/kg and <40-17,400 µg/kg, respectively). For the wider concentration ranges, higher RMSEP are expected, as the standard deviations in the extremes of the distribution are higher than in the centre. For that reason, to compare entirely the results obtained in all these studies, the same range of contamination should be used. As in our study, De Girolamo et al. (2014, 2009) also classified samples by LDA, in the first work applying a cut-off of 300 µg/kg, in which the classification accuracy was 69% and in the second work fixing a similar cut-off as in our study (1,200 µg/kg), in which a precision of 90% was obtained. Our poorer accuracies could be explained by the lower number of samples (150) than in both previous studies (394 and 464) and their concentration range. Moreover, different to preceding works using FT-NIR, we applied HSI-NIR directly in whole kernel samples, avoiding a previous grinding step. This technique could be, if refined, a rapid and cost-effective alternative to chemical analysis for screening of cereal batches according to DON contamination. This explains the difficulty to fit the model, due to the complex heterogeneity presented in whole samples in comparison to previously grinded ones.

Barbedo et al. (2017) published the first report using DON concentration as reference and HSI-NIR. Their initial experimental results revealed that direct estimation of DON content using HSI was currently unfeasible, but they also indicated that an indirect analysis exploiting the correlation between *Fusarium* damage and DON content may be accurate enough to improve the process of DON screening in the production chain. Thus they classified the wheat kernel batches into two or three categories, with accuracies of 81 and 72%, respectively. They worked with 251 naturally contaminated samples, from which 152 presented DON levels above 1250 µg/kg, well above our values. However, they analysed by

457 ELISA and liquid chromatography exactly the same grains as in the HIS-NIR system (once
458 images were captured), this point may be the key difference for their better performance,
459 and confirms that the variability of the different subsamples taken from the laboratory
460 sample for analysis is a key issue (as it is for chemical analysis). As a consequence, in
461 further studies it would be advisable to enlarge the size of the scanned samples and to
462 determine its optimum dimension. Barbedo et al. (2017) used 30-50 kernels and analysed
463 the scanned sample by ELISA/liquid chromatography in order to more accurately assess the
464 HIS-NIR performance. Our study presented differences in sampling conditions for the
465 qualitative analysis, in which each image contained approximately 200 kernels (7 g). In
466 addition, for kernel segmentation from the tray and the dark background, Barbedo et al.
467 (2015, 2017) operated on the 647 nm band to obtain the best contrast. Instead, we used
468 background segmentation based on the selection of similar pixels.

469 In our study no selection of wavelengths for the classification and regression models was
470 carried out, but we worked with the whole range, as this was just a starting point.
471 Interestingly, Barbedo et al. (2017) subtracted the reflectance at 623 nm from that at 1411
472 nm band, and worked with just one explanatory variable in the developed models. This was
473 done because it was observed that for healthy kernels these two bands did not differ much,
474 but they tended to diverge when DON was present. In our case, the results did not differ so
475 much when subtracting the lower weigh wavelengths, thus we decided to maintain the
476 whole NIR region. Other authors working on NIR spectrometry and *Fusarium*-damaged
477 wheat have related changes at 1420 nm to reduced water content (Barbedo et al., 2015), at
478 1200 nm to ergosterol levels (Dowell, Ram, & Seitz, 1999) and at 1480 nm to chitin levels
479 (Delwiche et al., 2011). A change near the 1450 nm is observed as a result of different
480 moisture contents (Sundaram, Mani, Kandala, & Holser, 2015). Fig. 5 showed two local
481 minimums at 1200 nm and 1450 nm that could be associated to ergosterol produced from
482 fungal cell and to the reduced water content in shrivelled kernels.

483 Recently, Liang et al. (2018) published a second research on DON detection in bulk wheat
484 kernels by HSI but at 400-1000nm, thus results are not comparable. However, a peak
485 appeared in 960 nm as in our reflectance raw spectra. They used naturally contaminated
486 grains (250-5000 μg/kg). They placed 70 overlapping wheat kernels in the scanning area
487 and, as in our case, recorded the mean spectra. The number of scanned kernels was reduced
488 in comparison with our study, in which approximately 200 kernels in triplicate were
489 examined. After an exhaustive search of the best preprocessing method for the data, as well
490 as for the selection of a discrete number of wavelengths (7 to 14) they achieved a 100%

classification (<250, 1162, 2655 μg/kg mean levels in each class) accuracy for the training set and 97.92% for the testing set. For each class, 44 images were used to calibrate the model and 16 images were used as a prediction dataset. Instead, we used 47 images to calibrate and 28 to obtain the accuracy for each classification group.

The remaining existing research works on HSI used visual appearance or FDK as reference variable, and used the mean spectra for individual kernels. In doing so, in the present work we observed that symptomatic and asymptomatic kernels were clearly discriminated by the HSI-NIR system in the PCA plots (Fig. 6). The possibility of using FDK to estimate DON levels was investigated by Paul, Lipps, & Madden (2005), with a correlation of 0.73. The PCA scores presented two well-defined groups, one on the left (contaminated and symptomatic) and one on the right (uncontaminated and asymptomatic). These groups corresponded to the positively correlated, in which the *Fusarium* infection have produced both kernel damage and DON on the kernel, corresponding to the 0.73 of the correlation. Otherwise, kernels with non-correlation between DON contamination and its symptomatology were represented in the middle of the score plot, in the region where both features converge and cannot be distinguished.

As stated before, HSI-NIR analysis has the ability to discriminate between FDK and non-FDK, and indirectly between DON contaminated and uncontaminated kernels, as both DON and symptomatology show a positive correlation. To go deep inside the evaluation of damage by the used technique, some studies using similar spectral range (900-1750 nm) to ours, have been compared (Polder, Van Der Heijden, Waalwijk, & Young, 2005). They worked with 96 artificially contaminated kernels and they also performed a quantification with HSI-NIR, but in this case, the reference values were obtained through TaqMan real-time PCR for *Fusarium* detection. A PLS model was built taking into account the spectra of complete grains, different from our mean spectra of the whole sample selection, leading to Q^2 levels of 0.42 (0.80 for highly contaminated grains). Similar Q^2 values were obtained by using the 1250/1050 nm reflectance ratio. The prediction performance cannot be compared, due to the wide differences in the methodology.

LDA classification methods were also used in previous works by Delwiche et al. (2010, 2011), but they were applied to FHB in samples instead of DON contamination, although they had the information on DON. As in our preliminary studies, they worked on mean spectra of crease-down positioned kernels. However, they selected 1199, 1474, 1315 nm and 1998 and 1486 (local minima or maxima), respectively, as wavelengths required for separation of kernels of healthy appearance from *Fusarium*-damaged kernels in LDA. Both

studies results presented correct classifications for high contrast in damage kernels but not for low contrast ones. This fact agrees with Fig. 6 in which the influence of the kernel symptomatology has more weight than DON contamination, although a correlation between both variables exists according to literature. However, Delwiche et al. (2010, 2011) used high DON contaminations (2900 to 13,500 µg/kg) in which *Fusarium* damage symptoms are expected. As in our study samples with low DON concentrations were used, visual symptoms in a high percentage of the kernels were not visually distinguishable (Barbedo et al., 2015). Thus, spectral pretreatments, algorithms construction, wavelength selections or more precise calibrations are needed to highlight DON influence above fungal damage on the NIR spectra.

Multivariate methods were applied also by Shahin & Symons (2011) work, in which PCA scores were used to extract six characteristic wavelengths by the loading plot to develop a LDA. Thus, Shahin & Symons (2012) used PLS to select the best wavelength combination (494, 578, 639, 678 nm) by regression coefficients which provided the higher accuracies for PLS-DA analysis. By contrast, we used a one-step LDA which assumes that the within-group covariance matrices are equal. High accuracies were achieved in both studies (92% and 90%, respectively), although their purpose was to classify between FDK and sound kernels and not between DON contaminated and uncontaminated samples. Additionally, individual kernel spectra collection was used, unlike sample mean selection achieved in our study.

The results of Barbedo et al. (2015) can be compared with our results (Fig. 6) regarding to the symptomatology of FDK. A 84% of correlation between DON contamination and visual assessment was achieved, thus this agrees with our results concerning PCA, in which kernels can be distinguished by both visual symptomatology and DON contamination. Although accurate correlations were achieved between DON/*Fusarium* Index, for low toxin contamination, visual symptoms were absent or too low to be visually assessed. Consequently, future studies are required for DON quantitative and qualitative analysis independent from imprecise visual evaluation. As in our work, kernel orientation was arranged randomly. Nevertheless, they analysed DON concentrations by LC-MS from kernels used in the hyperspectral images achieved previously, and not from kernels arising from the same sample, as in our case. Thus, their results would be more precise, as the sample heterogeneity can produce discordance between DON concentration in kernels achieved by the reference method and concentration in kernels scanned.

The high cost of NIR cameras may be a limiting factor in the development of commercially viable applications, and developing multispectral cameras may be more feasible than using hyperspectral ones. Moreover, the massive spectral variables and high dimensional data

require more time to process than other imaging systems. In addition, large amounts of data noise and redundant information exist in high-dimensional data, which reduce the prediction accuracy of the hyperspectral imaging data model (Elmasry, Kamruzzaman, Sun, & Allen, 2012). Thus, although in the present work the whole spectra were used, if better models were achieved, wavelength selection would be desirable. As described above, some authors chose a discrete number of wavelengths based on local spectra minima or maxima, and their differences related to visually damaged grains (Barbedo, Guarienti, & Tibola, 2018; Delwiche et al., 2010), other used PLS coefficients (Tekle, Mage, Segtnan, & Bjornstad, 2015) or used smarter techniques (Delwiche et al., 2019; Liang et al., 2018). In the NIR region, the lower wavelength region demonstrated closer similarity between sound and *Fusarium*-damaged kernels reflectance for most wavelengths pairs (Delwiche et al., 2011). The present work obtained high-influence regression coefficients by local minima or maxima selection in 955, 1287, 1403, 1455, 1528, 1671 and 1714 nm. The wavelength selection, especially the 1403 nm band is in accordance to Peiris, Pumphrey, & Dowell (2009) that observed DON absorptions in 1408 nm band. Previous studies highlight the importance, among others, of 950 nm (absorption from O-H) and 1400 nm (absorption from C-H) bands, which is related to scab effects on protein and starch and consequently the indirect detection of DON (Dowell et al., 1999). Moreover, a study of Delwiche & Gaines (2005) for the single wavelength sorting for *Fusarium*-damaged wheat stated that the best accuracy was obtained between 1450-1460 nm. These results are in accordance to some of our selected bands (955, 1403 and 1455 nm) with higher positive or negative coefficients of regression.

On the other hand, besides contaminated samples detection, this technique may have a great potential for cereal grain selection, detecting contaminated single kernels. In our preliminary trials, it was shown that single kernels from DON contaminated samples could be separated from those coming from samples showing no contamination, regardless of kernel location in the scanning area and kernel orientation (either crease-down or crease-up). In this work, the DON level was not analysed for each single kernel of the scanned sample, thus there is still room for improvement if grain selection was the aim. Similarly, a recent work (Delwiche et al., 2019) proposed HSI-NIR sorting of *Fusarium*-damaged kernels. They scanned about 200 kernels oriented at random for each sample, and 5 samples were used for model training, and 82 samples for model testing. Mean reflectance per kernel was calculated by averaging the pixel reflectances within the kernel. PLS-DA modelling was used to establish the limits of model accuracy for the evaluation of subsequent LDA models employing a much smaller number of wavelengths. From the 5

samples, a total of 278 sound and 278 damaged kernels were used. They selected 1100, 1197, 1308, and 1394 nm, with accuracies over 95% in the classification of the test kernels. Although still little studied, if sorting of grains by *Fusarium* damage/DON could be feasible, food safety management systems would not have to trust only the analytical screening for wheat batches admission, which has been shown to lack accuracy due to sampling variability. If HSI-NIR sorting could be implemented it would be a critical control measure that, in addition to improve food and feed safety, it would be more sustainable as only contaminated kernels and not whole batches would be diverted to other uses or for destruction.

5. CONCLUSION

A rapid and non-destructive method for the quantitative and qualitative analysis of DON is important for the mycotoxin management in cereals. The results obtained in the present work stated that HSI-NIR is a powerful technique for DON screening, as the preliminary outcomes confirmed the potential of this technique. The most significant parameters which can disturb DON discrimination have been evaluated and positive results have been accomplished. Moreover, the quantitative and qualitative analysis do not present high accuracy results for naturally contaminated samples, but these results are proposed as a starting point for further processing improvements and calibration techniques. Further studies will be required to improve HSI-NIR technique, as high-influence wavelength selection, reference method improvements or single kernel quantification. Additionally, new methodologies to overcome sample heterogeneity are necessary to obtain high accurate classification and low prediction error results. Notwithstanding those hitches, the initial results are encouraging, thus the HSI-NIR is proposed as a prospective system for DON quantification and kernel sorting for DON reduction.

6. CONFLICTS OF INTEREST

The authors declare that they have no conflict of interest.

7. AKNOWLEDGEMENTS

The authors are grateful to the University of Lleida (predoctoral grant), and to the Spanish Ministry of Science, Innovation and Universities (Project AGL2017-87755-R) for funding this work.

8. REFERENCES

AOAC. (2005). Official Methods of Analysis. *Official Methods of Ananlysis of AOAC International*, *18*, 20877–22417.

Barbedo, J. G. A., Guarienti, E. M., & Tibola, C. S. (2018). Detection of sprout damage in wheat kernels using NIR hyperspectral imaging. *Biosystems Engineering*, *175*, 124–132. https://doi.org/10.1016/j.biosystemseng.2018.09.012

Barbedo, J. G. A., Tibola, C. S., & Fernandes, J. M. C. (2015). Detecting Fusarium head blight in wheat kernels using hyperspectral imaging. *Biosystems Engineering*, *131*, 65–76. https://doi.org/10.1016/j.biosystemseng.2015.01.003

Barbedo, J. G. A., Tibola, C. S., & Lima, M. I. P. (2017). Deoxynivalenol screening in wheat kernels using hyperspectral imaging. *Biosystems Engineering*, *155*, 24–32. https://doi.org/10.1016/j.biosystemseng.2016.12.004

Beyer, M., Klix, M. B., & Verreet, J. A. (2007). Estimating mycotoxin contents of *Fusarium*-damaged winter wheat kernels. *International Journal of Food Microbiology*, *119*(3), 153–158. https://doi.org/10.1016/j.ijfoodmicro.2007.07.007

Cano-Sancho, G., Valle-Algarra, F. M., Jiménez, M., Burdaspal, P., Legarda, T. M., Ramos, A. J., … Marín, S. (2011). Presence of trichothecenes and co-occurrence in cereal-based food from Catalonia (Spain). *Food Control*, *22*(3–4), 490–495. https://doi.org/10.1016/j.foodcont.2010.09.033

Caporaso, N., Whitworth, M. B., & Fisk, I. D. (2018). Near-Infrared spectroscopy and hyperspectral imaging for non-destructive quality assessment of cereal grains. *Applied Spectroscopy Reviews*, *53*(8), 667–687. https://doi.org/10.1080/05704928.2018.1425214

Cen, H., Lu, R., Zhu, Q., & Mendoza, F. (2016). Nondestructive detection of chilling injury in cucumber fruit using hyperspectral imaging with feature selection and supervised classification. *Postharvest Biology and Technology*, *111*, 352–361. https://doi.org/10.1016/j.postharvbio.2015.09.027

De Girolamo, A., Cervellieri, S., Visconti, A., & Pascale, M. (2014). Rapid analysis of deoxynivalenol in durum wheat by FT-NIR spectroscopy. *Toxins*, *6*(11), 3129–3143. https://doi.org/10.3390/toxins6113129

De Girolamo, A., Lippolis, V., Nordkvist, E., & Visconti, A. (2009). Rapid and non-invasive analysis of deoxynivalenol in durum and common wheat by Fourier-Transform Near Infrared (FT-NIR) spectroscopy. *Food Additives & Contaminants: Part A*, *26*(6), 907–917. https://doi.org/10.1080/02652030902788946

Delwiche, S. R., Kim, M. S., & Dong, Y. (2010). Damage and quality assessment in wheat by NIR hyperspectral imaging. In M. S. Kim, S.-I. Tu, & K. Chao (Eds.), *Sensing for Agriculture and Food Quality and Safety II* (Vol. 7676, pp. 1–8). https://doi.org/10.1117/12.851150

Delwiche, S. R., Kim, M. S., & Dong, Y. (2011). *Fusarium* damage assessment in wheat kernels by Vis/NIR hyperspectral imaging. *Sensing and Instrumentation for Food Quality and Safety*, *5*(2), 63–71. https://doi.org/10.1007/s11694-011-9112-x

Delwiche, S. R., Rodriguez, I. T., Rausch, S. R., & Graybosch, R. A. (2019). Estimating percentages of *Fusarium*-damaged kernels in hard wheat by near-infrared hyperspectral imaging. *Journal of Cereal Science*, *87*, 18–24. https://doi.org/10.1016/j.jcs.2019.02.008

Dowell, F. E., Ram, M. S., & Seitz, L. M. (1999). Predicting scab, vomitoxin, and ergosterol in single wheat kernels using near-infrared spectroscopy. *Cereal Chemistry*, *76*(4), 573–576. https://doi.org/10.1094/CCHEM.1999.76.4.573

Dvořáček, V., Prohasková, A., Chrpová, J., & Štočková, L. (2012). Near infrared spectroscopy for deoxynivalenol content estimation in intact wheat grain. *Plant, Soil and Environment*, *58*(4), 196–203.

Edwards, S. G., & Jennings, P. (2018). Impact of agronomic factors on *Fusarium* mycotoxins in harvested wheat. *Food Additives & Contaminants: Part A*, *35*(12), 2443–2454. https://doi.org/10.1080/19440049.2018.1543954

Elmasry, G., Kamruzzaman, M., Sun, D., & Allen, P. (2012). Principles and applications of hyperspectral imaging in quality evaluation of agro-food products: a review. *Critical Reviews in Food Science and Nutrition*, *52*(11), 999–1023. https://doi.org/10.1080/10408398.2010.543495

Femenias, A., Gatius, F., Ramos, A. J., Sanchis, V., & Marín, S. (2020). Use of hyperspectral imaging as a tool for *Fusarium* and deoxynivalenol risk management in cereals : A review. *Food Control*, *108*(August 2019), 106819. https://doi.org/10.1016/j.foodcont.2019.106819

K. H. S. Peiris, Y. Dong, W. W. Bockus, & F. E. Dowell. (2013). Estimation of Bulk Deoxynivalenol and Moisture Content of Wheat Grain Samples by FT-NIR Spectroscopy. In *2013 Kansas City, Missouri, July 21 - July 24, 2013*. St. Joseph, MI: American Society of Agricultural and Biological Engineers. https://doi.org/10.13031/aim.20131593402

Liang, K., Liu, Q. X., Xu, J. H., Wang, Y. Q., Okinda, C. S., & Shena, M. X. (2018). Determination and visualization

of different levels of deoxynivalenol in bulk wheat kernels by hyperspectral imaging. *Journal of Applied Spectroscopy*, *85*(5), 953–961. https://doi.org/10.1007/s10812-018-0745-y

Paul, P. A., Lipps, P. E., & Madden, L. V. (2005). Relationship between visual estimates of Fusarium Head Blight intensity and deoxynivalenol accumulation in harvested wheat grain: A meta-analysis. *Phytopathology*, *95*(10), 1225–1236. https://doi.org/10.1094/PHYTO-95-1225

Peiris, K. H. S., Pumphrey, M. O., & Dowell, F. E. (2009). NIR Absorbance characteristics of deoxynivalenol and of sound and *Fusarium*-damaged wheat kernels. *Journal of Near Infrared Spectroscopy*, *17*(4), 213–221. https://doi.org/10.1255/jnirs.846

Polder, G., Van Der Heijden, G. W. A. M., Waalwijk, C., & Young, I. T. (2005). Detection of *Fusarium* in single wheat kernels using spectral imaging. *Seed Science and Technology*, *33*(3), 655–668. https://doi.org/10.15258/sst.2005.33.3.13

S. R. Delwiche, & C. S. Gaines. (2005). Wavelength selection for monochromatic and bichromatic sorting of Fursarium-damaged wheat. *Applied Engineering in Agriculture*, *21*(4), 681–688. https://doi.org/10.13031/2013.18557

Shahin, M. A., & Symons, S. J. (2011). Detection of *Fusarium* damaged kernels in Canada Western Red Spring wheat using visible/near-infrared hyperspectral imaging and principal component analysis. *Computers and Electronics in Agriculture*, *75*(1), 107–112. https://doi.org/10.1016/j.compag.2010.10.004

Shahin, M. A., & Symons, S. J. (2012). Detection of *Fusarium* damage in Canadian wheat using visible/near-infrared hyperspectral imaging. *Journal of Food Measurement & Characterization*, *6*(1–4), 3–11. https://doi.org/10.1007/s11694-012-9126-z

Sundaram, J., Mani, S., Kandala, C. V. K., & Holser, R. A. (2015). Application of NIR Reflectance Spectroscopy on Rapid Determination of Moisture Content of Wood Pellets. *American Journal of Analytical Chemistry*, *06*(12), 923–932. https://doi.org/10.4236/ajac.2015.612088

Tekle, S., Mage, I., Segtnan, V. H., & Bjornstad, A. (2015). Near-infrared hyperspectral imaging of *Fusarium*-damaged oats (Avena sativa L.). *Cereal Chemistry*, *92*(1), 73–80. https://doi.org/10.1094/CCHEM-04-14-0074-R

Vidal, A., Sanchis, V., Ramos, A. J., & Mar??n, S. (2016). The fate of deoxynivalenol through wheat processing to food products. *Current Opinion in Food Science*, *11*, 34–39. https://doi.org/10.1016/j.cofs.2016.09.001

Vidal, A., Sanchis, V., Ramos, A. J., & Marín, S. (2018). Stability of DON and DON-3-glucoside during baking as affected by the presence of food additives. *Food Additives and Contaminants - Part A Chemistry, Analysis, Control, Exposure and Risk Assessment*, *35*(3), 529–537. https://doi.org/10.1080/19440049.2017.1401741

Williams, P. J., Geladi, P., Britz, T. J., & Manley, M. (2012). Near-infrared (NIR) hyperspectral imaging and multivariate image analysis to study growth characteristics and differences between species and strains of members of the genus *Fusarium*. *Analytical and Bioanalytical Chemistry*, *404*(6–7), 1759–1769. https://doi.org/10.1007/s00216-012-6313-z

Xing, F., Yao, H., Liu, Y., Dai, X., Brown, R. L., & Bhatnagar, D. (2019). Recent developments and applications of hyperspectral imaging for rapid detection of mycotoxins and mycotoxigenic fungi in food products. *Critical Reviews in Food Science and Nutrition*, *59*(1), 173–180. https://doi.org/10.1080/10408398.2017.1363709

Figure captions

Fig. 1. a) Hyperspectral image of 30 wheat kernels in crease-down orientation. b) Hyperspectral image of 7 g of wheat (approximately 200 kernels).

Fig. 2. Evaluation of the differences between kernel position on the scanning tray.

Fig. 3. PCA score plot of the 3 different scans of the same kernels placed in different positions on the tray. X-expl: 94%, 5%. N=90.

Fig. 4. Mean spectra profile of 30 crease-down kernel samples at three DON concentrations. B = <LOD; M = 1605.9 μg/kg; C = 2682.8 μg/kg.

728 Fig. 5. Evaluation of the influence of the kernel position on the ability of HSI-NIR to
729 discriminate between DON-contaminated and <LOD kernels. Result 1 = X-expl: 97%; 1%.
730 Result 2 = X-expl: 99%; 1%. Result 3 = X-expl: 98%; 1%. N = 120.

731 Fig. 6. Evaluation of the influence of the kernel symptomatology on the ability of HSI-NIR to
732 discriminate between DON-contaminated and <LOD kernels. CS = Contaminated/Symptomatic;
733 CA = Contaminated/Asymptomatic; BS = Non-contaminated/Symptomatic; BA = Non-
734 contaminated/Asymptomatic. Xexpl: 97%, 1%.

735 Fig. 7. PCA score plot for four bulk samples subsampled three times and scanned (7 g) in
736 triplicate (Mean of triplicated scans are presented). Baseline corrected absorbance spectra. X-
737 expl: 100%, 0%. N=12.

738 Fig. 8. Predicted vs. measured plot for PLS calibration set. Optimum number of PC: 17. N =
739 200

740 Fig. 9. Predicted vs. measured plot for PLS validation set. Optimum number of PC: 12. N = 150.

741

Training set				Validation set			
	Predicted		Accuracy (%)		Predicted		Accuracy (%)
Groups	B	C		Groups	B	C	
B	33	14	73.4	B	33	14	62.7
C	6	22		C	14	14	

742 ***Table 1. Linear discriminant analysis (LDA) accuracies for training and validation sets.***

743 B = low-contaminated group of samples (< 1250 µg/kg); C = contaminated group of
744 samples (> 1250 µg/kg). Grey cells indicate the number of correctly-classified samples.
745 White cells indicate the number of miss-classified samples.

Figure 1

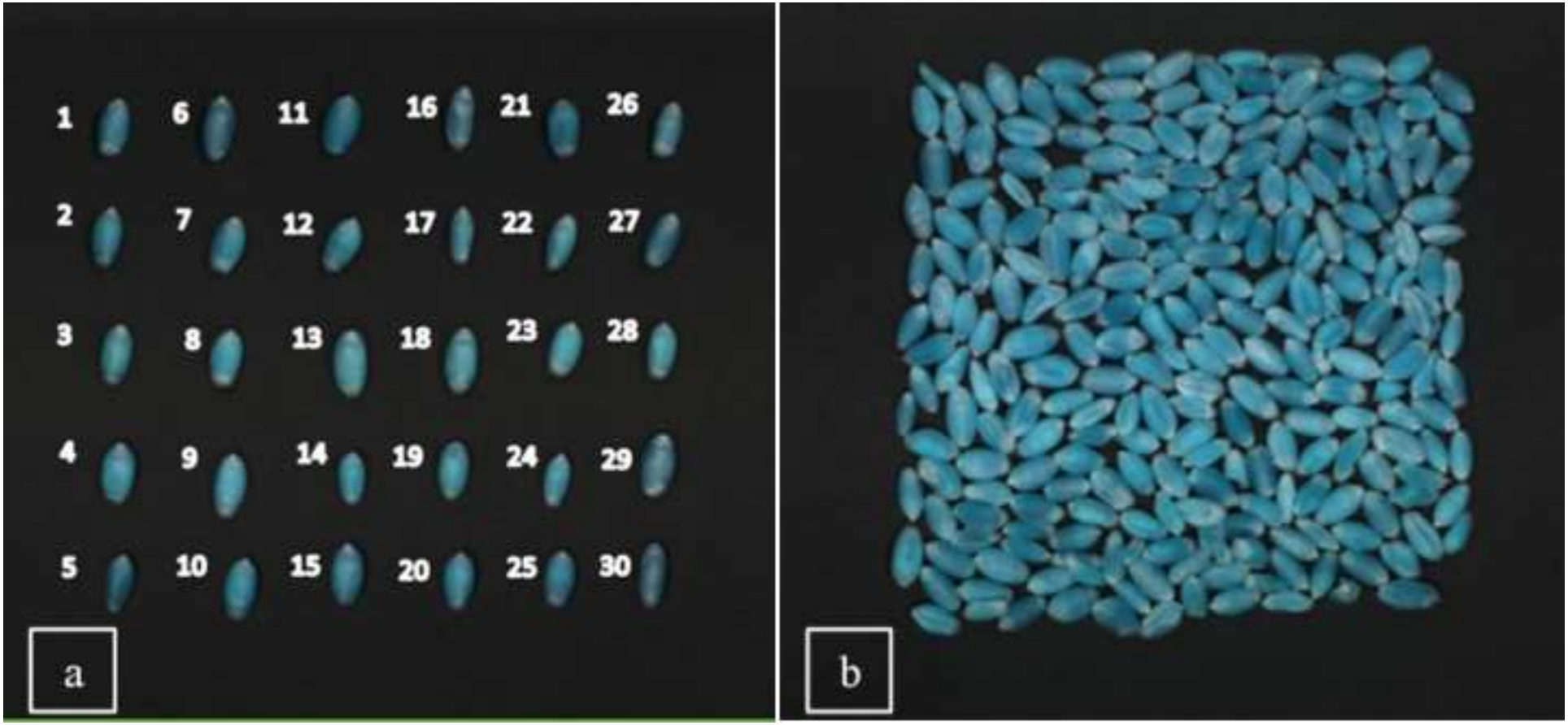
1 6 11 16 21 26
2 7 12 17 22 27
3 8 13 18 23 28
4 9 14 19 24 29
5 10 15 20 25 30
a
b

Figure 2


1 6 11 16 21 26
2 7 12 17 22 27
3 8 13 18 23 28
4 9 14 19 24 29
5 10 15 20 25 30
26 21 16 11 6 1
27 22 17 12 7 2
28 23 18 13 8 3
29 24 19 14 9 4
30 25 20 15 10 5
30 25 20 15 10 5
29 24 19 14 9 4
28 23 18 13 8 3
27 22 17 12 7 2
26 21 16 11 6 1

Figure 3

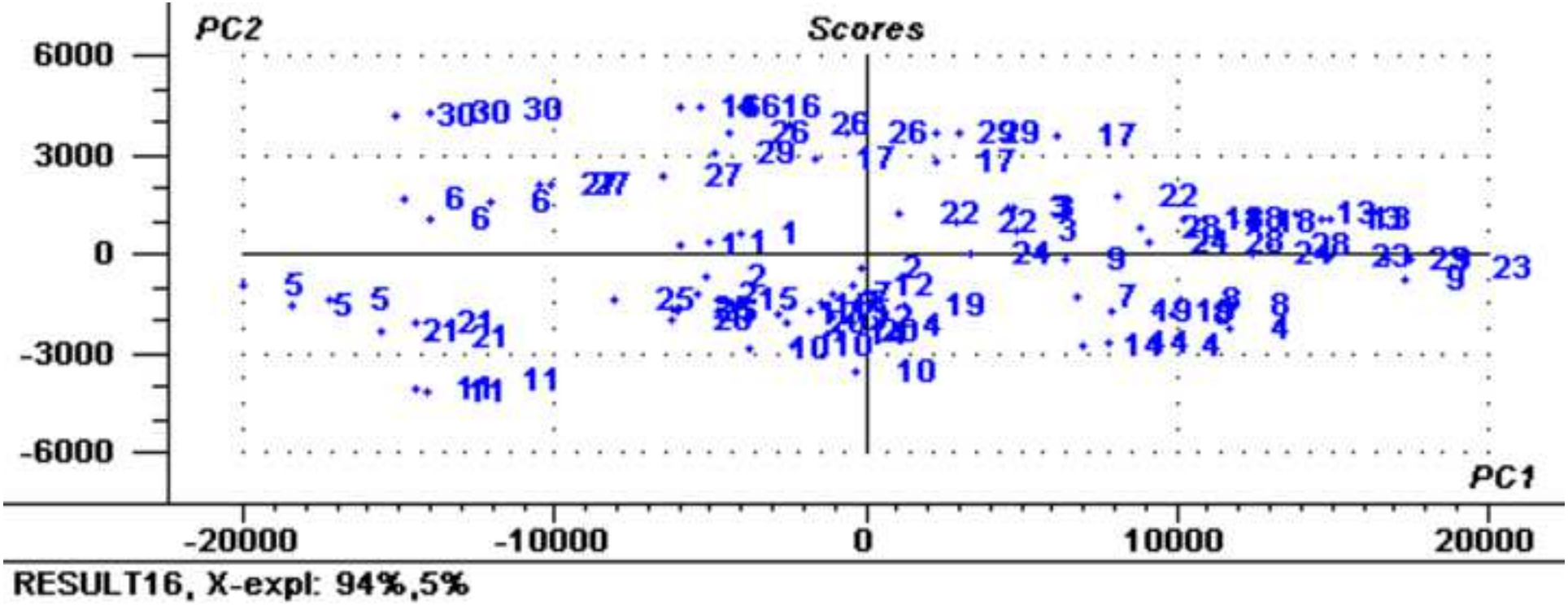
PC2
Scores
6000
3000
0
-3000
-6000
PC1
-20000
-10000
0
10000
20000
RESULT16, X-expl: 94%,5%

Figure 4

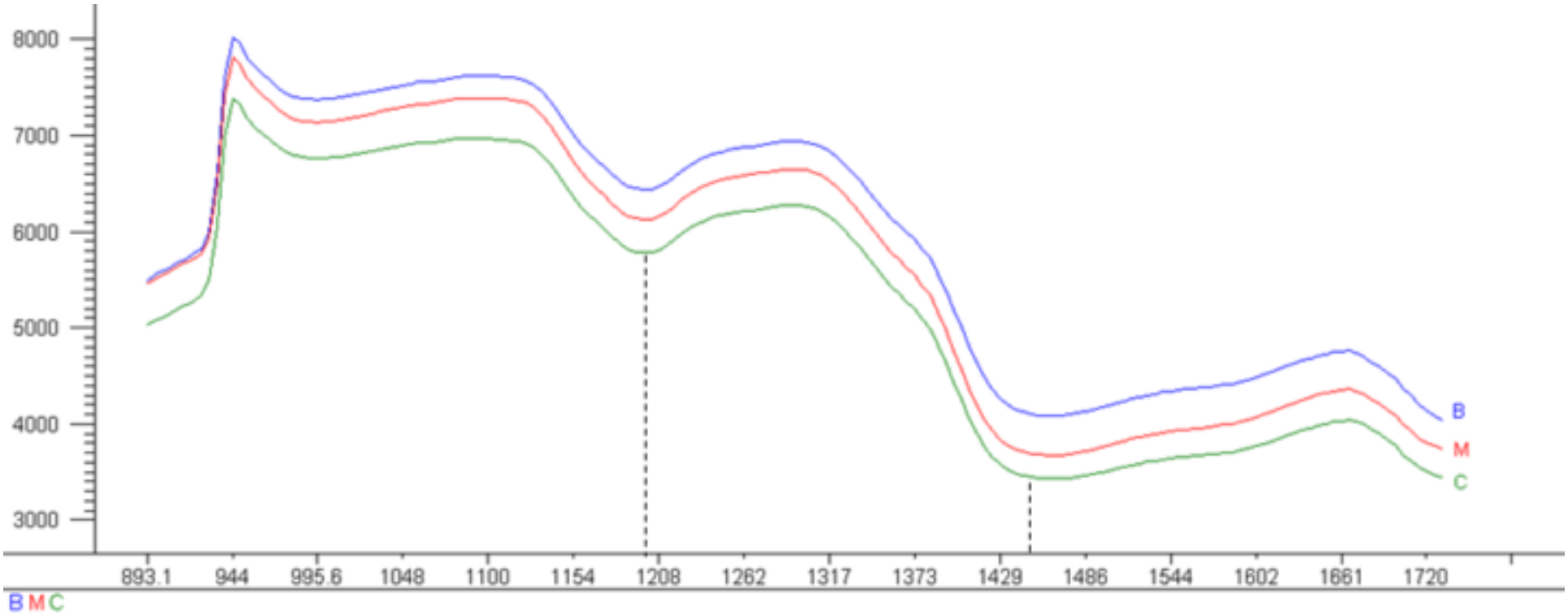
8000
7000
6000
5000
4000
3000
893.1
944
995.6
1048
1100
1154
1208
1262
1317
1373
1429
1486
1544
1602
1661
1720
B
M
C
B M C

Figure 5

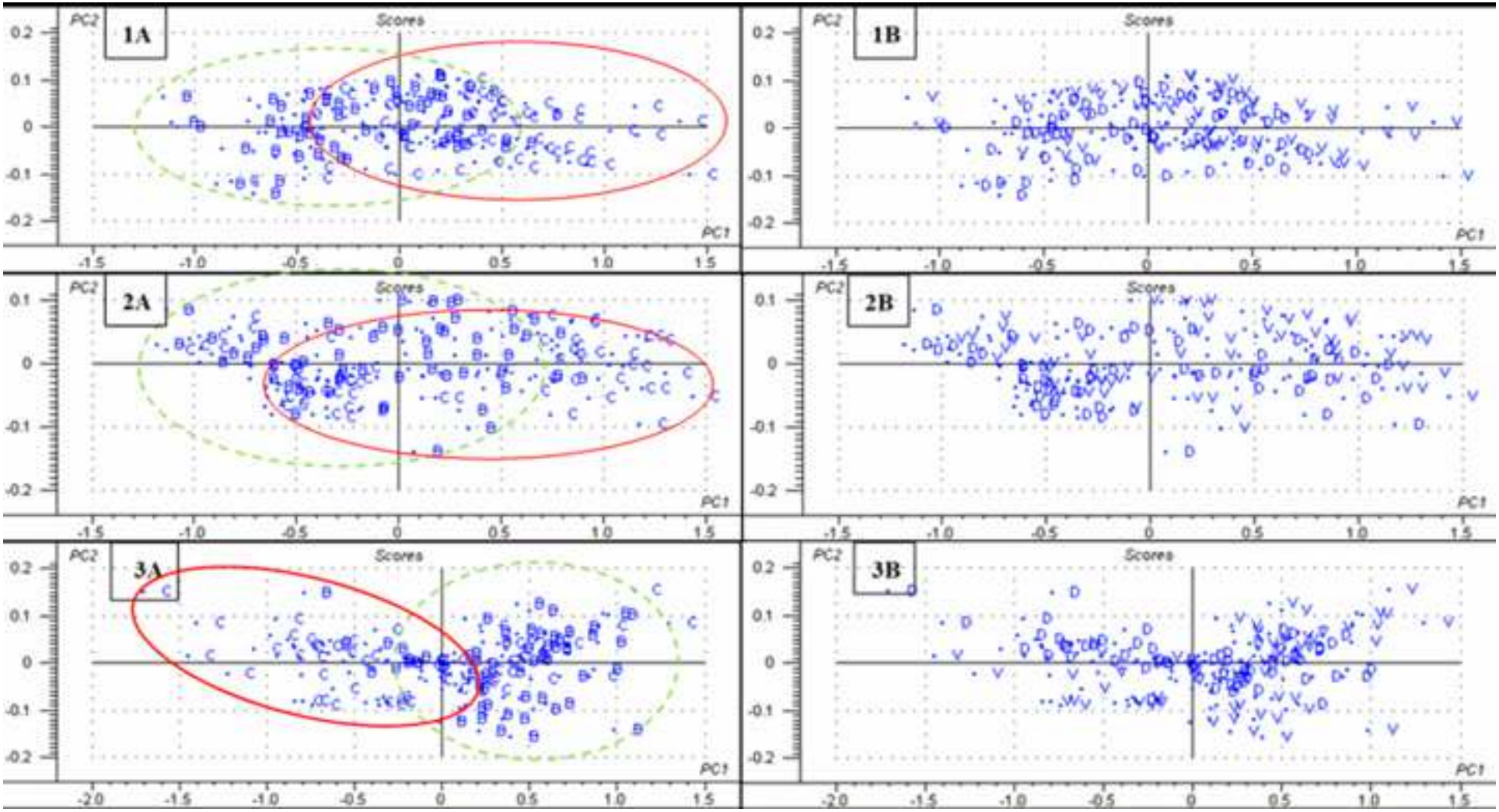

Figure 6

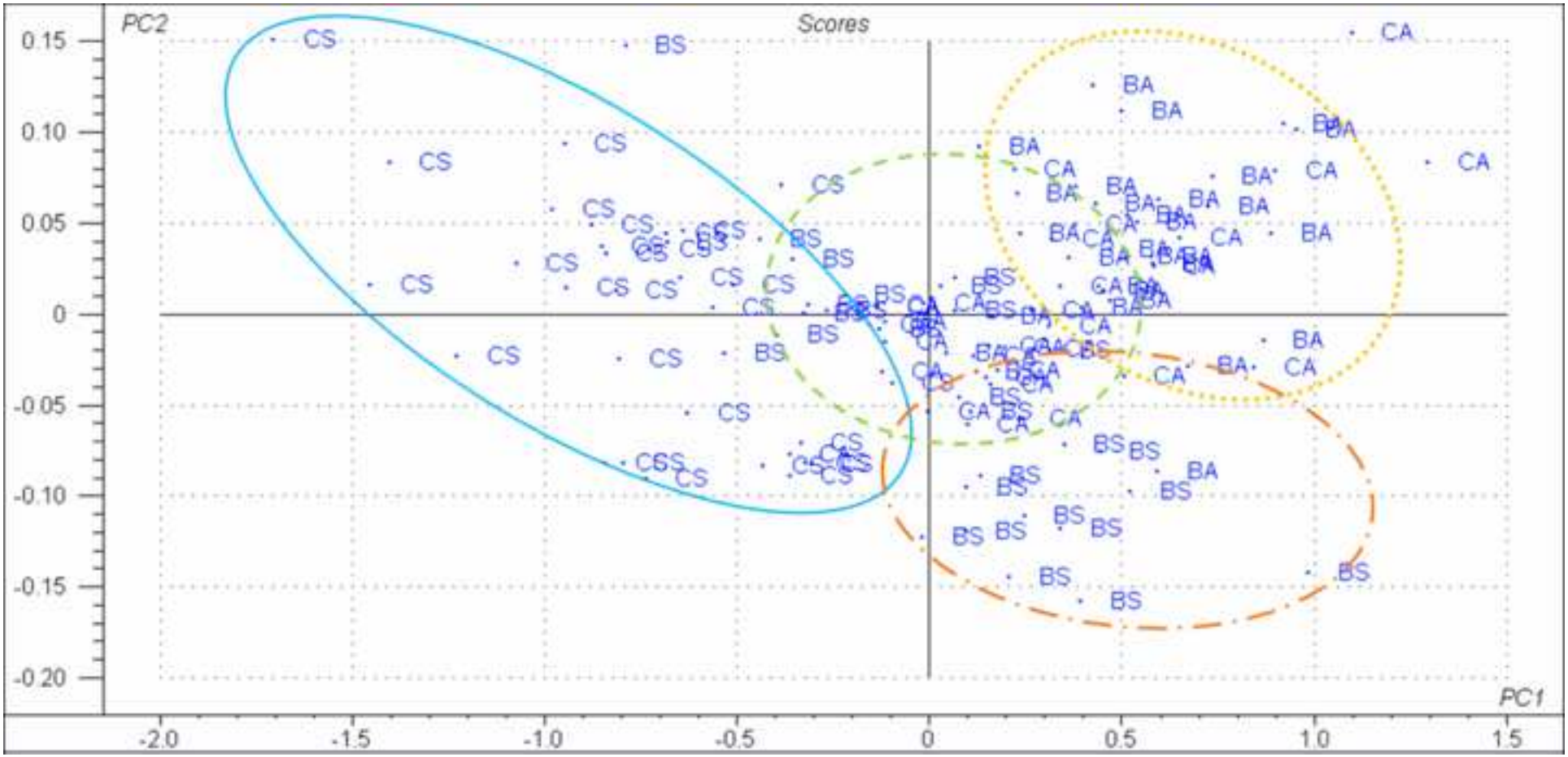
Scores
PC2
PC1
0.15
0.10
0.05
0
-0.05
-0.10
-0.15
-0.20
-2.0
-1.5
-1.0
-0.5
0
0.5
1.0
1.5
CS
BS
BA
CA

Figure 7

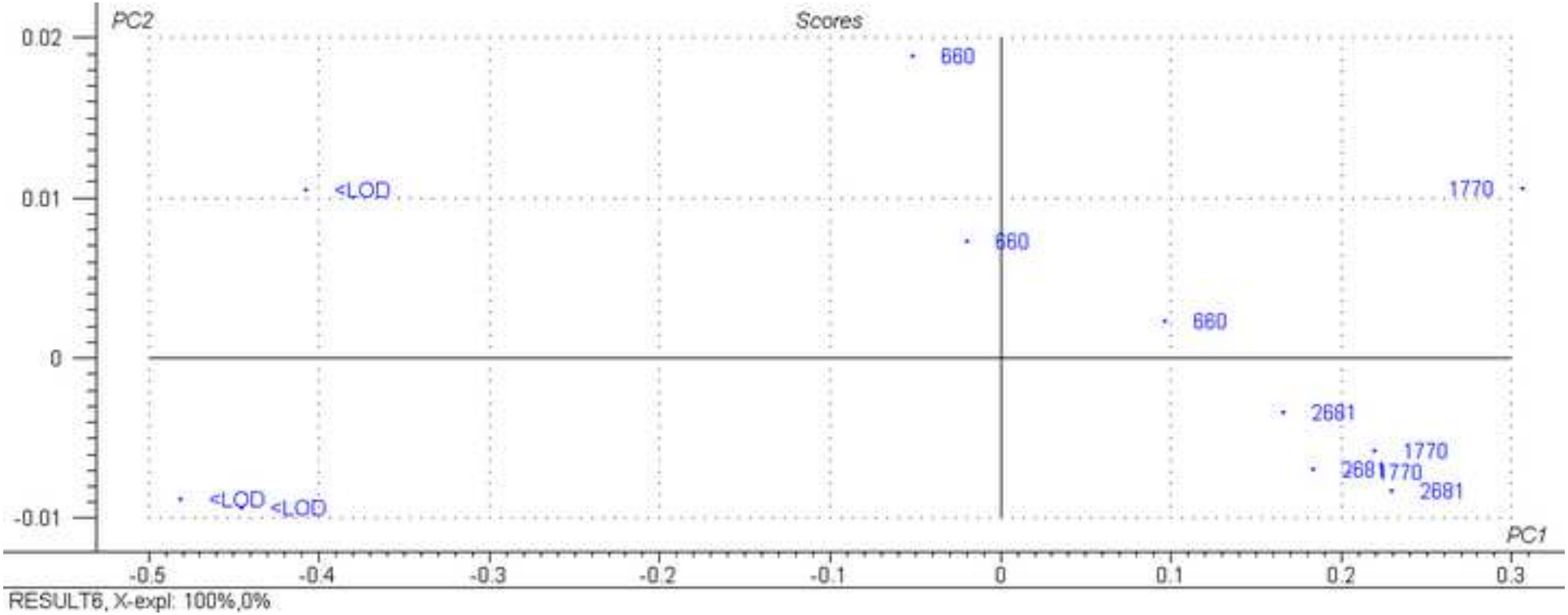
PC2
Scores
0.02
0.01
0
-0.01
660
<LOD
660
1770
660
2681
1770
2681
1770
<LOD
<LOD
PC1
-0.5
-0.4
-0.3
-0.2
-0.1
0
0.1
0.2
0.3
RESULT6, X-expl: 100%,0%

Figure 8

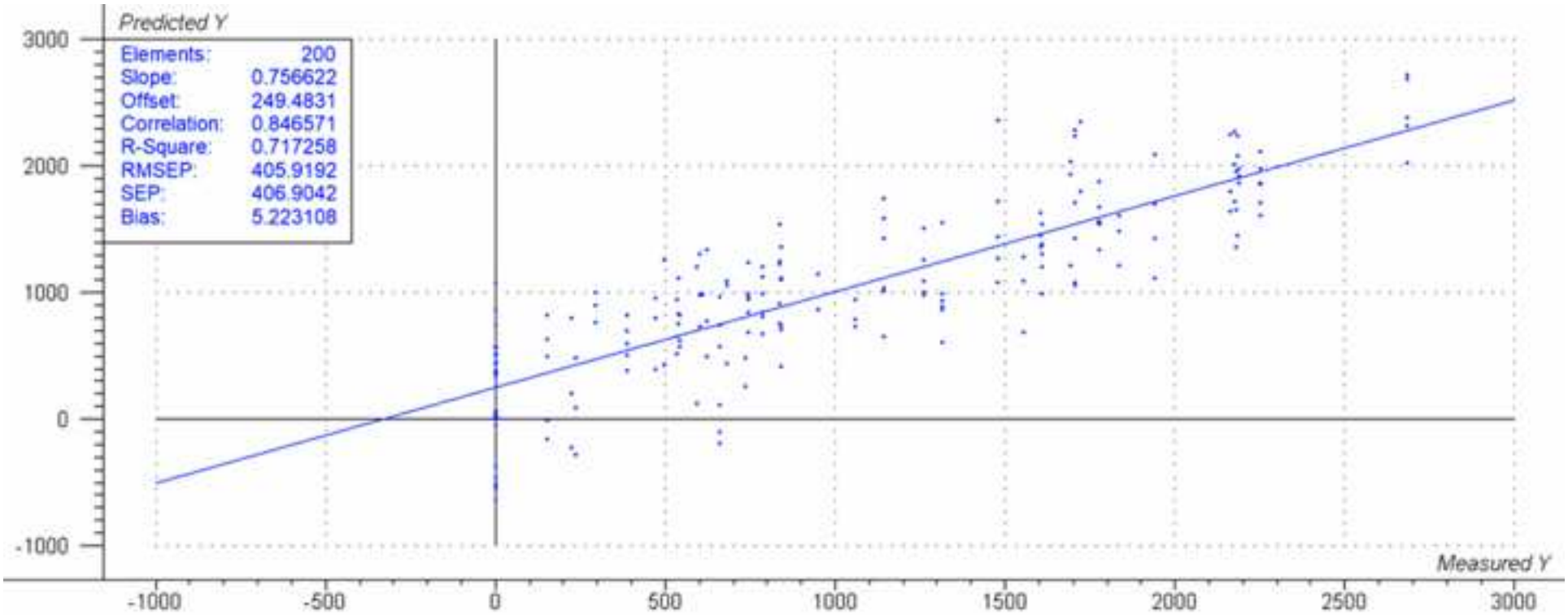
Predicted Y
Elements: 200
Slope: 0.756622
Offset: 249.4831
Correlation: 0.846571
R-Square: 0.717258
RMSEP: 405.9192
SEP: 406.9042
Bias: 5.223108
3000
2000
1000
0
-1000
-1000
-500
0
500
1000
1500
2000
2500
3000
Measured Y

Figure 9

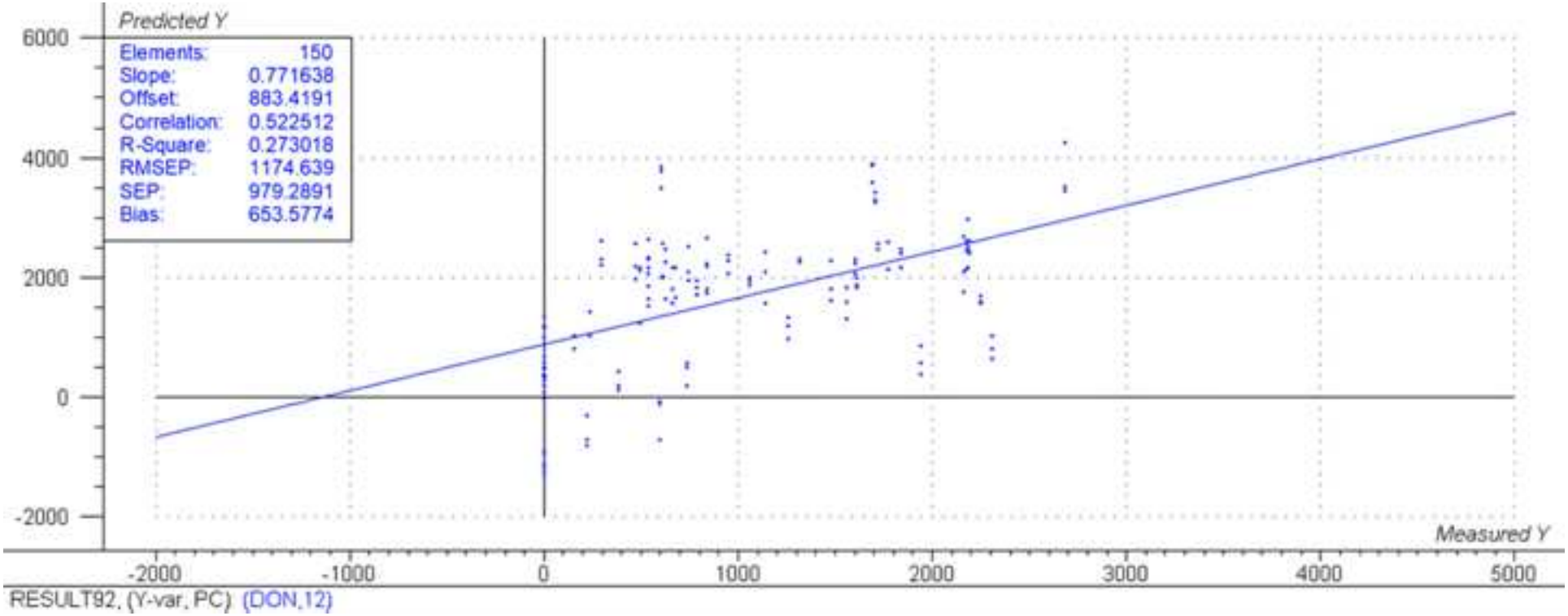
Predicted Y
Elements: 150
Slope: 0.771638
Offset: 883.4191
Correlation: 0.522512
R-Square: 0.273018
RMSEP: 1174.639
SEP: 979.2891
Bias: 653.5774
6000
4000
2000
0
-2000
-2000
-1000
0
1000
2000
3000
4000
5000
Measured Y
RESULT92, (Y-var, PC) (DON,12)

SUPPLEMENTARY MATERIAL

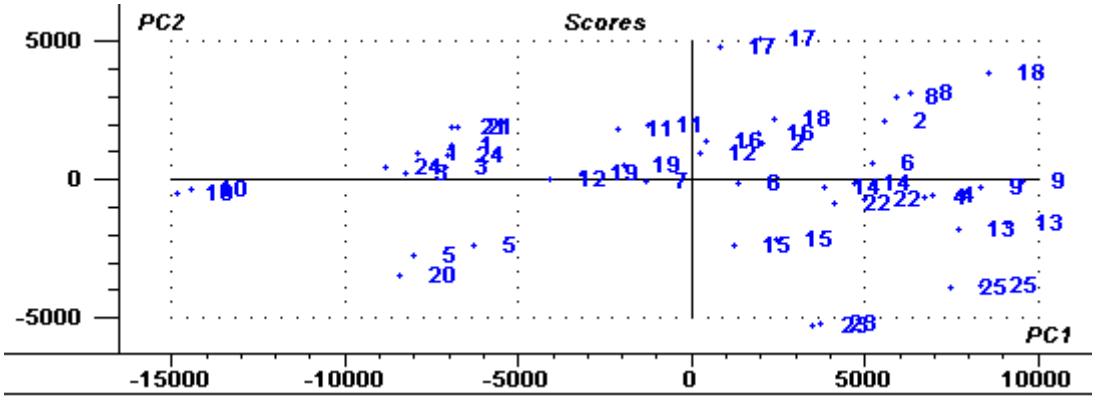

Fig. S1. PCA score plot for the assessment of the repeatability of the pixel selection option. X-expl: 88%, 11%. N=50.

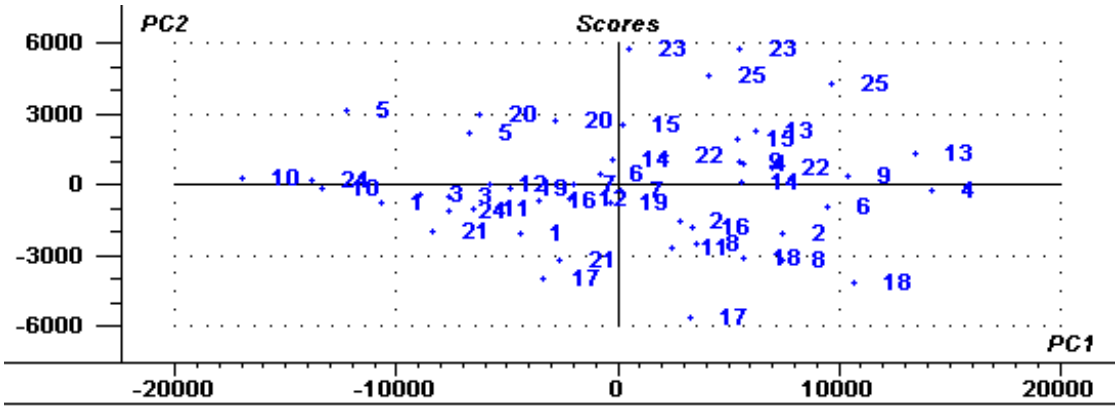

Fig. S2. PCA score plot for the representation of the differences between narrow and wider pixel selection options. X-expl: 89%, 10%. N=50.

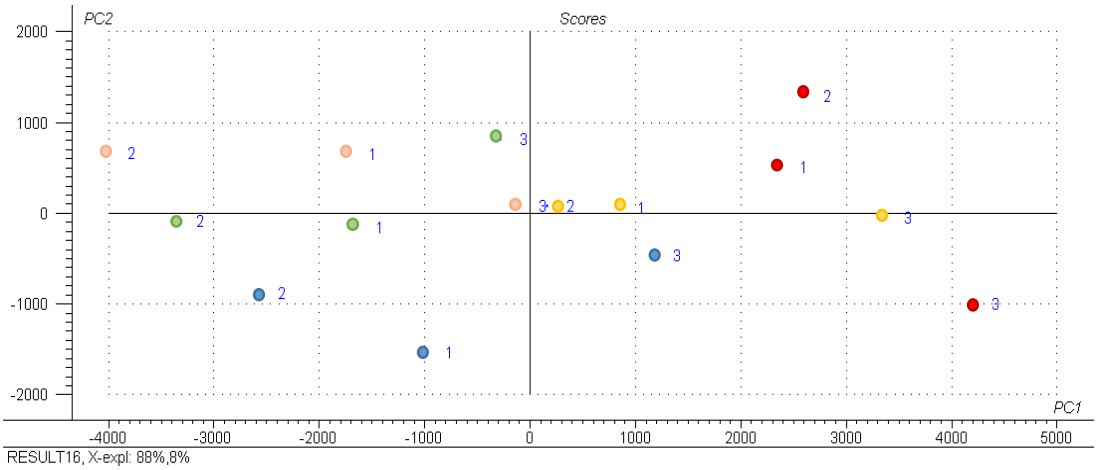

Fig. S3. PCA score plot for the assessment of the interday repeatability. Five samples were scanned in three different days. Raw spectra. 1=1st day scan; 2=2nd day scan; 3=3rd day scan. X-expl: 88%, 8%. N=15.

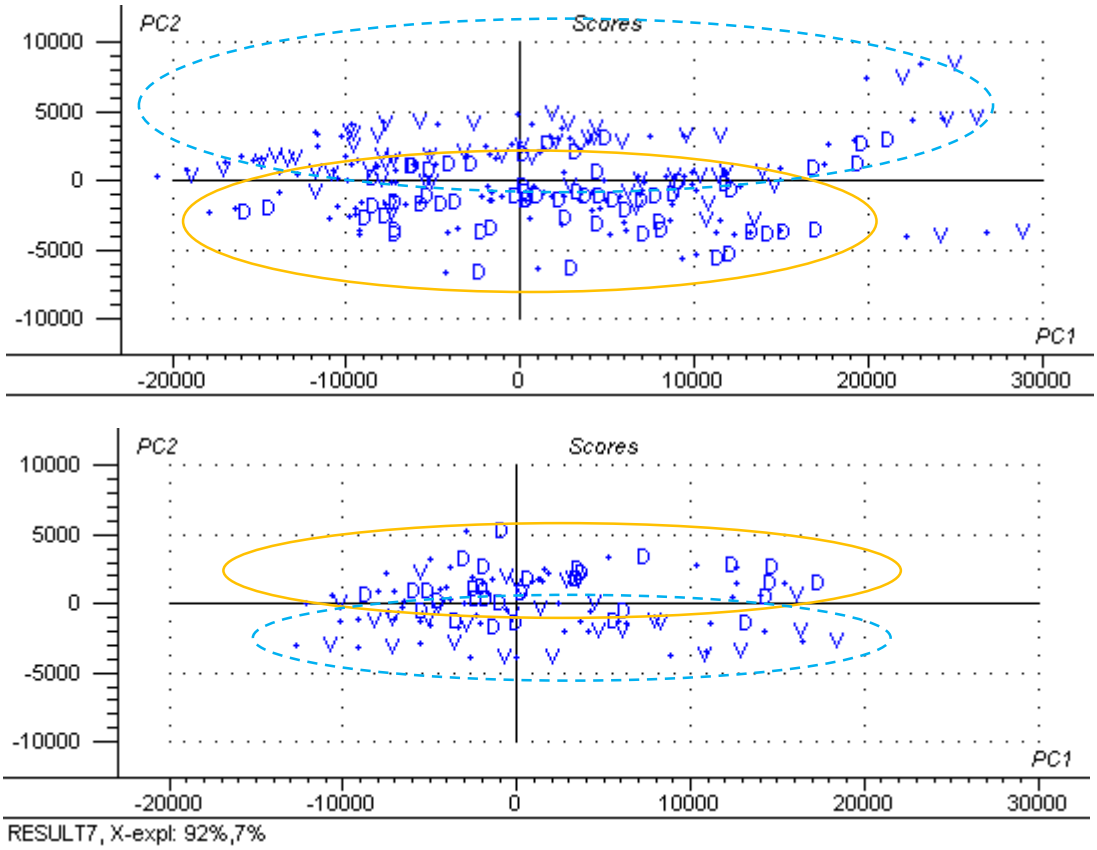

Fig. S4. PCA score plot of the differences between crease-down/up kernel position for a DON-free sample (upper, X-expl: 93%, 7%. N=60) and a DON-contaminated sample (lower, X-expl: 92%, 7%. N=60). D = Crease down (Dorsal), V = Crease-up (Ventral).

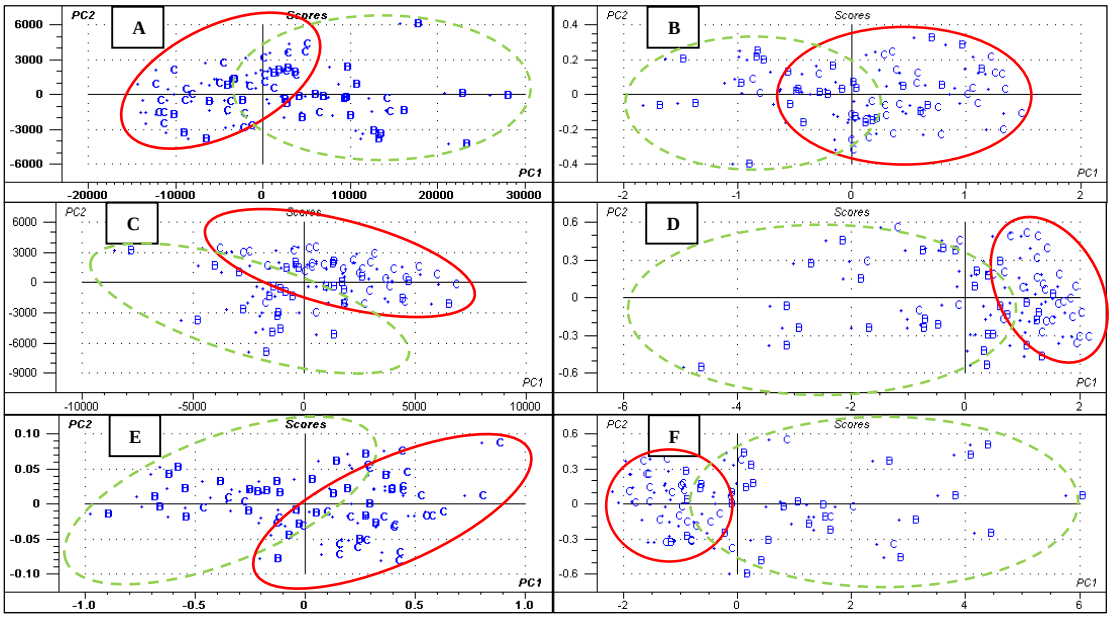

Fig. S5. Comparison between spectral pretreatments for crease-down positioned kernels. A = Raw spectra (reflectance) X-expl: 95%, 5%; B = Raw spectra (absorbance) X-expl: 95%, 4%; C = Reflectance + Baseline correction X-expl: 58%, 40%; D = Reflectance + SNV X-expl: 91%, 3%; E = Absorbance + Baseline correction X-expl: 98%, 1%; F = Absorbance + SNV X-expl: 94%, 2%. N = 60.

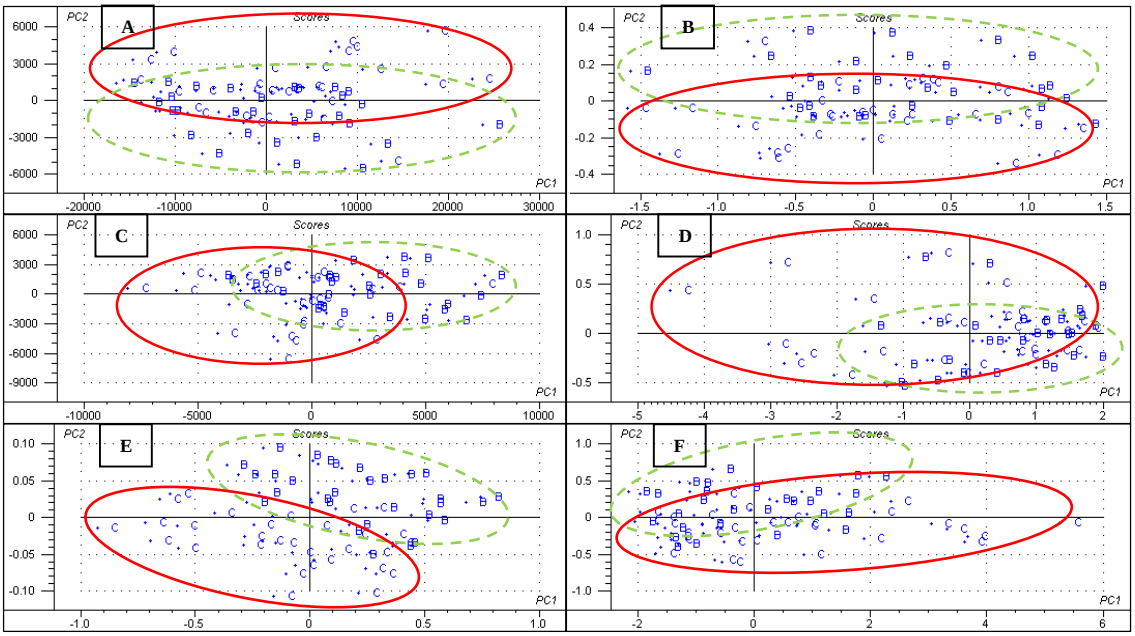

Fig. S6. Comparison between spectral pretreatments for crease-up positioned kernels. A = Raw spectra (reflectance) X-expl: 93%, 6%; B = Raw spectra (absorbance) X-expl: 94%, 5%; C = Reflectance + Baseline correction X-expl: 66%, 31%; D = Reflectance + SNV X-expl: 88%, 5%; E = Absorbance + Baseline correction X-expl: 97%, 2%; F = Absorbance + SNV X-expl: 91%, 3%. N = 60.